Role of Tryptophan 161 in Catalysis by Human Manganese Superoxide Dismutase†

Diane E. Cabelli,*,‡ Yue Guan,§ Vincent Leveque,|| Amy S. Hearn,|| John A. Tainer,§ Harry S. Nick,|| and David N. Silverman*,||

Chemistry Department, Brookhaven National Laboratory, Upton, New York 11973-5000, Department of Molecular Biology, The Scripps Research Institute, 10550 North Torrey Pines Road, La Jolla, California 92037, and Departments of Pharmacology, Biochemistry, and Neuroscience, University of Florida, Gainesville, Florida 32610-0267

Received April 22, 1999; Revised Manuscript Received June 30, 1999

ABSTRACT: Tryptophan 161 is a highly conserved residue that forms a hydrophobic side of the active site cavity of manganese superoxide dismutase (MnSOD), with its indole ring adjacent to and about 5 Å from the manganese. We have made a mutant containing the conservative replacement Trp 161 → Phe in human MnSOD (W161F MnSOD), determined its crystal structure, and measured the catalysis of the resulting mutant using pulse radiolysis to produce $O_2^{\bullet-}$. In the structure of W161F MnSOD the phenyl side chain of Phe 161 superimposes on the indole ring of Trp 161 in the wild type. However, in the mutant, the hydroxyl side chain of Tyr 34 is 3.9 Å from the manganese, closer by 1.2 Å than in the wild type. The tryptophan in MnSOD is not essential for the half-cycle of catalytic activity involving reduction of the manganese; the mutant W161F MnSOD had k_{cat}/K_m at 2.5×10^8 M^{-1} s^{-1}, reduced only 3-fold compared with wild type. However, this mutant exhibited a strong product inhibition with a zero-order region of superoxide decay slower by 10-fold compared with wild type. The visible absorption spectrum of W161F MnSOD in the inhibited state was very similar to that observed for the inhibited wild-type enzyme. The appearance of the inhibited form required reaction of 2 molar equiv of $O_2^{\bullet-}$ with W161F Mn(III)SOD, one to form the reduced state of the metal and the second to form the inhibited complex, confirming that the inhibited complex requires reaction of $O_2^{\bullet-}$ with the reduced form of the enzyme. This work suggests that a significant role of Trp 161 in the active site is to promote the dissociation of product peroxide, perhaps in part through its effect on the orientation of Tyr 34.

Manganese superoxide dismutase (MnSOD)[1] catalyzes the disproportionation of superoxide, $O_2^{\bullet-}$, to form dioxygen and hydrogen peroxide protecting mitochondria from oxidative damage. It is well accepted that the pathway for this catalysis proceeds through reactions in which manganese cycles between oxidized and reduced states (*1*, *2*).

$$P{-}Mn^{3+} + O_2^{\bullet-} \underset{k_{-1}}{\overset{k_1}{\rightleftharpoons}} [P{-}Mn^{3+}{-}O_2^{\bullet-}] \xrightarrow{k_2} P{-}Mn^{2+} + O_2 \quad (1)$$

$$P{-}Mn^{2+} + O_2^{\bullet-} + 2H^+ \underset{k_{-3}}{\overset{k_3}{\rightleftharpoons}} [P{-}Mn^{2+}{-}O_2^{\bullet-}] + 2H^+ \underset{k_{-4}}{\overset{k_4}{\rightleftharpoons}} P{-}Mn^{3+} + H_2O_2 \quad (2)$$

$$k_5 \updownarrow k_{-5}$$

$$P{-}Mn^{3+}{-}X$$

Here $P{-}Mn^{3+}$ represents manganese bound in the enzyme. The rate of this catalysis measured by pulse radiolysis for *Bacillus stearothermophilus* MnSOD (*3*) and human MnSOD (*4*) and by stopped-flow spectrophotometry for MnSOD from *Thermus thermophilus* (*5*) shows an initial burst of catalysis followed by a region of apparent enzyme inhibition that is zero-order in superoxide (observed for $[O_2^{\bullet-}]/[E_0] \gtrsim 10$). In the simplest catalytic scheme (*3*), individual steps of the catalysis are irreversible, but the enzyme can reversibly interconvert between an active and inactive form. In more complex schemes (*5*), the individual steps are reversible, and the inactive enzyme, represented as $P{-}Mn^{3+}{-}X$ in eq 2, is again suggested to form reversibly. The zero-order rate is determined, in part, by the rate constant for the return of the inactive form to a species in the catalytic cycle, described as k_{-5} of eq 2 (*3*, *5*). Bull et al. (*5*) observed the visible absorption spectrum of the enzyme during the zero-order phase of catalysis and, on the basis of comparison to spectra of inorganic complexes, suggested that the inhibited complex is a side-on peroxo complex of Mn(III)SOD resulting from the oxidative addition of $O_2^{\bullet-}$ to Mn(II)SOD. Another possibility is that inhibition occurs by the conversion of an outer- to an inner-sphere complex of product peroxide with the manganese (*1*).

Human MnSOD is a homotetramer of 22 kDa subunits; the crystal structure at 2.2 Å resolution shows that the geometry about the metal is trigonal bipyramidal with

† This work was supported by grants from the National Institutes of Health, GM 54903 (to D.N.S.) and GM 48495 (to J.A.T.), and by American Cancer Society Fellowship 1-36-97B (to Y.G.). The pulse radiolysis work was carried out at Brookhaven National Laboratory under Contract DE-AC02-98CH108816 with the Department of Energy and supported by its Division of Chemical Sciences, Office of Basic Energy Sciences.

* Address correspondence to D.N.S., Box 100267 Health Center, University of Florida, Gainesville, FL 32610-0267 (phone 352-392-3556; fax 352-392-9696; e-mail silvrmn@nervm.nerdc.ufl.edu), or D.E.C., Chemistry Department, Brookhaven National Laboratory, P.O. Box 5000, Upton, NY 11973-5000 (phone 516 344-4361; fax 516 344-5815; e-mail cabelli@bnl.gov).

‡ Brookhaven National Laboratory.

§ The Scripps Research Institute.

|| University of Florida.

[1] Abbreviations: MnSOD, manganese superoxide dismutase; Mops, 3-(*N*-morpholino)propanesulfonic acid; Taps, 3-[[tris(hydroxymethyl)-methyl]amino]propanesulfonic acid; Ches, 2-(cyclohexylamino)ethanesulfonic acid; RMSD, root-mean-square deviation.

10.1021/bi9909142 CCC: $18.00
Published on Web 08/17/1999

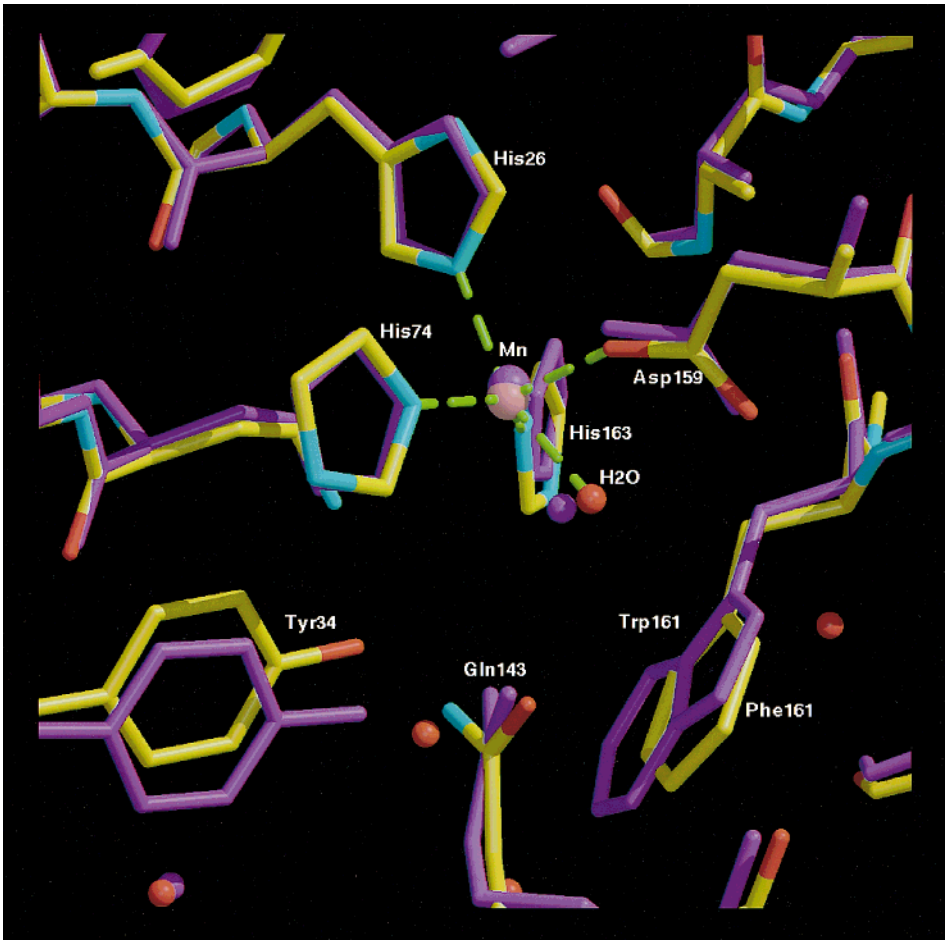

FIGURE 1: Structure of the active site of human W161F MnSOD (multicolored) showing the conformation of Phe 161 with respect to the manganese and other active site residues from the crystal structure at 2.3 Å resolution. Superimposed is the structure of the wild-type MnSOD (purple) [from the data of Borgstahl et al. (*6*)].

coordination to three histidines, a monodentate aspartate, and a solvent molecule (Figure 1) (*6*). The enzyme is purified predominantly in the oxidized form, Mn(III)SOD. The replacement by mutagenesis of three prominent nonliganded residues at the active site for either MnSOD or FeSOD shows that these three residues contribute to catalysis but are not essential: His 30 (*7*), Tyr 34 (*8*−*11*), and Gln 143 (12). Another prominent residue is Trp 161, which forms one side of the active site cavity with the metal adjacent to the plane of its aromatic ring and with the manganese 5.6 Å from the Nϵ of the indole ring of Trp 161. The crystal structure of the wild type shows the manganese-bound aqueous ligand extending into the active site cavity with the metal−oxygen bond pointing directly toward the side chain of Trp 161 and with its oxygen 4.0 Å from the Nϵ of the indole ring (*6*).

We report here the structural and catalytic properties of W161F human MnSOD, the mutant containing the replacement Trp 161 → Phe. This mutant has been crystallized in the orthorhombic crystal form homologous to the wild type (*6*), and its crystal structure has been determined to 2.3 Å resolution with an R-factor of 22.7% (R_{free} 30%). Using pulse radiolysis, we have determined that Trp 161 is not essential for catalysis in the reduction half-cycle of eq 1. Its replacement by Phe results in a mutant with strong catalytic activity only 3−4-fold less than wild type. However, this mutant is much more strongly product inhibited than the wild type or any other mutant of MnSOD studied to date. This provides useful information on the properties of the inhibited state and the pathway of its formation.

METHODS

Preparation and Purification of Enzymes. The oligonucleotides GCATATGAAGCACAGCCTCC and GGAGATCTCAGCATAACGATC were used as primers for PCR to amplify the human MnSOD cDNA [cDNA sequence reported by Beck et al. (*13*)]. The plasmid pHMNSOD4 (ATCC 59947) which contains human MnSOD was subcloned into the TA cloning vector, pCRII (Invitrogen Corp.). Four primers were designed in order to create the mutant W161F. First, we designed a pair of oligonucleotides, primer 1 (5′ CGCTAGTAATCATTTCATGAAGCACAGCCTCCCC G 3′) and primer 2 (5′ CTGCAGAATACAGTAAGCTGC 3′) which, through PCR, would recreate the entire MnSOD coding region. Second, we prepared two oligonucleotides designated primer 3 (5′ GGG ATT GAT GTG TTC GAA CAC GCT TAC 3′) and primer 4 (5′ GTA AGC GTG TTC GAA CAC ATC AAT CCC 3′), whose sequences are complementary to each other and code for a phenylalanine at position 161 (underlined). Two separate PCR reactions were used to amplify the 5′ half (primers 1 and 4) and 3′ half (primers 3 and 2) of the MnSOD cDNA coding sequence. The PCR products from these two reactions were purified using electroelution and used as template DNA for the second round of PCR using primers 1 and 2. The human

W161F MnSOD PCR product was cloned into the expression vector pTrc 99A (Pharmacia Corp.). Cloning was accomplished by using the restriction sites *Bsp*HI and *Pst*I incorporated into primers 1 and 2, respectively. The *Bsp*HI site, which corresponds to the N-terminal portion of the protein, was annealed to the compatible cohesive ends of the *Nco*I site in pTrc 99A, recreating an ATG codon. The C-terminal end of the cDNA was cleaved and reannealed to pTrc 99A using *Pst*I. The mutation was verified by DNA sequencing, along with the remainder of the coding sequence. This construct expressed human MnSOD as a mature protein in the mutant SodA/SodB *Escherichia coli* [strain QC774 (*14*)] and tagged with an extra methionine at the amino terminus. Culture conditions included 100 μM $MnCl_2$. Yields of human MnSOD mutant protein were on average 70 mg of protein/50 g of bacterial pellet.

The W161F mutant protein was purified from *E. coli* using a combination of heat treatment (60 °C), dialysis, and ion-exchange chromatography (DE52 and CM52) according to the procedures of Beck et al. (*15*). The purity of the resulting samples was determined on SDS−polyacrylamide gels which showed a single intense band. The metal content of the mutant enzyme was measured by atomic absorption spectroscopy. In all of our calculations, the concentration of enzyme is taken as the manganese concentration determined in this manner. The fraction of active sites occupied by manganese was determined to be near 80%. Protein concentrations were determined by the Lowry method.

Crystallography. Rod-shaped crystals of W161F MnSOD were grown from solutions consisting of 22 mg/mL protein buffered in 25 mM K_2HPO_4 and 22% poly(ethylene glycol) (PEG) 2000 monomethyl ether. Crystals belong to the orthorhombic crystal form which is homologous to the native human MnSOD crystals with a space group of $P2_12_12$ and unit cell dimensions of $a = 74.0$ Å, $b = 77.2$ Å, and $c = 67.8$ Å. One flash-cooled W161F crystal was mounted under a liquid N_2 stream, and data were collected using the Siemens SRA rotating anode X-ray generator with a MAR345 area detector. The data were processed using DENZO (*16*) and the R_{sym} was 6.4% to 2.3 Å resolution (46.8% for the last bin). The total number of unique reflections was 17 730. The structure of the W161F mutant was refined with CNS (*17*) using one dimer of human MnSOD as an initial model. A dimeric W161F model in the asymmetric unit was first rigid-body refined followed by geometry-restrained positional refinement. The model was further simulated, annealing refined by heating to 3000 K and gradually cooling followed by temperature factor refinement in CNS (*17*). The model was refit to σA weighted $2F_o - F_c$ and $F_o - F_c$ maps using Xfit (*18*). The refinement was completed using a bulk solvent correction in X-PLOR (*19*) with the manganese ion completely unrestrained during the final round of refinement to remove any force field bias. The final model consists of two W161F subunits and 166 solvent molecules with an *R*-factor of 22.7%.

Pulse Radiolysis. The pulse radiolysis experiments were carried out using the 2 MeV van de Graaff accelerator at Brookhaven National Laboratory. Dosimetry was established using the KSCN dosimeter, assuming that $(SCN)_2^-$ has a *G* value of 6.13 and a molar absorptivity of 7950 M^{-1} cm^{-1} at 472 nm (*20*). All UV/vis spectra were recorded on a Cary 210 spectrophotometer thermostated at 25 °C. The path length was either 2.0 or 6.1 cm. The actual concentration of manganese in MnSOD was determined from atomic absorption using a Pye-Unicam AA instrument. The reported rate constants for the MnSOD studies are based on manganese concentration and not MnSOD concentration, with the assumption that all of the metal is bound and active and behaves independently from the other metal centers. Solutions contained enzyme, 30 mM sodium formate [as a hydroxyl radical scavenger (*21*)], 50 μM EDTA, and 2 mM buffer: Mops (pH 7.2), Taps (pH 8.2), or Ches (pH 9.2). Superoxide radicals (1−20 μM) were generated upon pulse radiolysis of an aqueous, air/O_2 saturated solution containing sodium formate according to the mechanisms described by Schwarz (*21*). Under our conditions, the formation of O_2^-/HO_2 radicals is more than 90% complete by the first microsecond after the pulse. Changes in absorbance of superoxide (*22*) or enzyme were observed spectrophotometrically.

Scanning Stopped-Flow Spectrophotometry. Reactions of superoxide and wild-type or W161F MnSOD were observed by scanning stopped-flow spectrophotometry (Applied Photophysics Ltd., SX.18MV) in a sequential mixing experiment in which KO_2 in a solution of dimethyl sulfoxide and 18-crown-6 (*23*) was diluted in two sequential rapid mixings resulting in a final solution containing 0.50 mM enzyme, 0.95 mM $O_2^{\bullet-}$, 1.0 mM EDTA, and 100 mM Ches buffer at pH 9.1. To attain a sufficiently large final concentration of $O_2^{\bullet-}$ (near 1 mM), the initial solution of KO_2 was not greatly diluted and the final solution after mixing contained 14% dimethyl sulfoxide by volume.

RESULTS

Crystal Structure. The overall tetrameric structure of W161F closely resembles the conformation of the native human MnSOD with an overall RMSD for Cα's of 0.37 Å. By comparing the detailed wild-type and W161F structures, we found that the side chain of Phe 161 superimposed on that of Trp 161 in the active site. The hydroxyl of Tyr 34 was shifted 1.2 Å in W161F, placing this side chain much closer to the metal in the mutant compared with the wild type (Figure 1). The Mn−OH(Tyr 34) distance was 3.9 Å in the mutant and 5.1 Å in the wild type, which places the side chain of Tyr 34 in a more prominent position in the active site of the mutant from which it may influence catalysis or inhibition. Phe 66 and His 30 were also more shifted toward the metal in the mutant. The driving force comes from the smaller side chain of Phe 161 compared to Trp 161. The geometry about the manganese shows that the coordination distances in the mutant are slightly longer, by approximately 0.2 Å, than in the native structure.

Catalysis. In experiments using pulse radiolysis to generate superoxide, the change in absorbance of superoxide in the presence of the mutant W161F MnSOD showed an initial decrease followed by a plateau of apparent enzyme inhibition (Figure 2). This pattern of an initial catalysis followed by a region of zero-order decay of $O_2^{\bullet-}$ is characteristic of wild-type MnSOD, both for the bacterial (*3, 5*) and for the human MnSOD (*4*). However, in the case of W161F MnSOD the slope of the zero-order region of apparent inhibition is smaller than in wild type; that is, there is less turnover of $O_2^{\bullet-}$ for the mutant, suggesting more complete inhibition of the

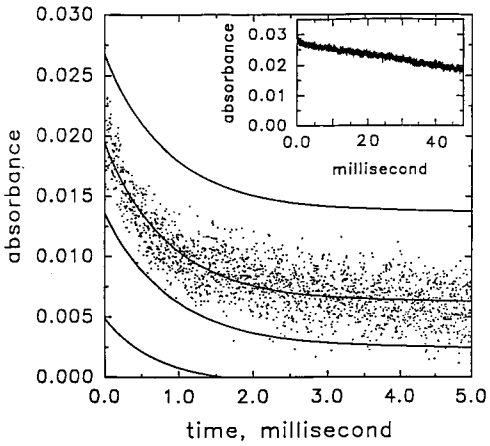

FIGURE 2: Decrease in absorbance at 260 nm of superoxide in the presence of 3.9 μM W161F MnSOD measured by pulse radiolysis. Solutions contained 30 mM formate, 50 μM EDTA, and 2 mM Taps at pH 8.2 and 25 °C. Initial concentrations of superoxide were (from top) 7.0, 5.1, 3.4, and 1.0 μM. The solid lines are least-squares fits to first-order kinetics with rate constants of (from top) 1.4×10^3 s^{-1}, 1.1×10^3 s^{-1}, 1.1×10^3 s^{-1}, and 1.1×10^3 s^{-1}. Experimental points are shown for just one experiment to simplify the figure. Inset: Decrease in absorbance at 260 nm for the initial concentration of superoxide at 7.0 μM with time extended to 50 ms. Other conditions were the same.

Table 1: Values of the Steady-State Parameters for the Decay of Superoxide Catalyzed by Human MnSOD and Mutants

enzyme	k_{cat} (s^{-1})	k_{cat}/K_m (μM^{-1} s^{-1})	$k_0/[E_0]$ (s^{-1})
wild type[a]	40000	800	500
Y34F[a]	3300	870	80
W161F[b]	>1000[c]	250	50
Q143N[d]	300	0.82	—[e]

[a] pH 9.4 and 20 °C from Guan et al. (*11*). [b] pH 9.2 and 25 °C; this work. [c] K_m is large for this mutant, and we were not able to increase superoxide to values large enough to measure k_{cat}. [d] pH 9.4 and 5 °C from Hsieh et al. (*12*). [e] No zero-order region of enzyme inhibition was observed with this mutant.

enzyme. The inset to Figure 2 shows a typical pulse radiolysis measurement of catalysis by W161F MnSOD extending to longer times. The zero-order rate constant $k_0/[E_0] = 50$ s^{-1} was observed at pH 8.2 and 9.2; at pH 7.2 it was measured at 110 s^{-1}. Table 1 compares values of $k_0/[E_0]$ from wild type, W161F MnSOD, and other mutants at pH 9.2−9.6.

Another estimate of the enhanced product inhibition of the mutant W161F MnSOD was obtained by scanning stopped-flow spectrophotometry. The appearance of the inhibited complex of wild-type MnSOD is characterized by an absorbance maximum near 420 nm ($\epsilon_{420} \approx 400$ M^{-1} cm^{-1}) that decays to the weak and featureless visible absorption spectrum of Mn(II)SOD as catalysis proceeds (*5*). Under comparable conditions in a scanning stopped-flow experiment, W161F MnSOD showed much stronger evidence than wild type for the presence of the inhibited state, as indicated by the larger absorbance at 420 nm (Figure 3). These data are consistent with the enhanced inhibited phase of catalysis in W161F compared with wild-type MnSOD observed by pulse radiolysis in Figure 2 and Table 1.

The initial rate of decay of superoxide in the presence of W161F MnSOD was measured in a range of initial concentrations of superoxide varying from 1 to 20 μM (typical data in Figure 2). Measuring initial velocities gave an estimate

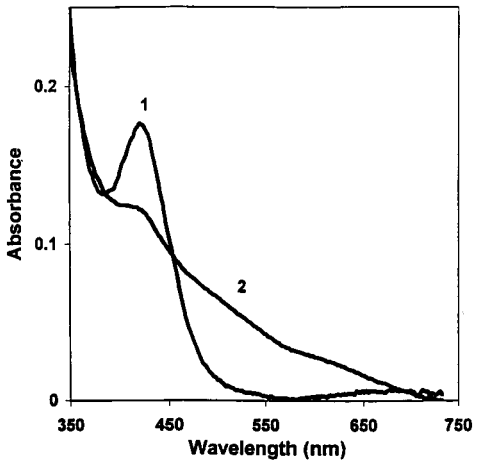

FIGURE 3: Scanning stopped-flow spectra of (1) W161F human MnSOD and (2) wild-type human MnSOD both 5.2 ms after mixing with 0.95 mM $O_2^{\bullet-}$. The final solution after mixing contained 14% DMSO used to introduce superoxide. The enzyme concentrations were 0.50 mM in solutions containing 1 mM EDTA and 100 mM Ches at pH 9.1 and 20 °C.

of $k_{cat}/K_m = 2.5 \times 10^8$ M^{-1} s^{-1}, which was found to be independent of pH in a range from pH 7.2 to pH 9.2. This is somewhat less than the value of 8×10^8 M^{-1} s^{-1} found for k_{cat}/K_m with wild-type human MnSOD (*4*). A comparison with values of k_{cat}/K_m for other mutants is given in Table 1.

Product Inhibition. Wild-type Mn(II)SOD can be obtained by reduction of the oxidized form with superoxide as in eq 1 or with H_2O_2 (*3*). Unlike its analogue FeSOD, which is inactivated by reaction with H_2O_2, MnSOD does not undergo Fenton-type chemistry with hydrogen peroxide. The result that MnSOD is not inactivated with H_2O_2 is consistent with earlier reports of McAdam et al. (*24*) and more recent studies of Yamakura et al. (*25*). The resulting Mn(II)SOD has a very weak visible absorption spectrum with $\epsilon < 50$ M^{-1} cm^{-1} and no peaks. We used pulse radiolysis to generate superoxide and measured the reaction of $O_2^{\bullet-}$ with W161F MnSOD in the reduced state. The amount of superoxide consumed at each pulse was determined from the difference of the extrapolated values of the final and the initial superoxide concentrations. When the amount of superoxide reacted was plotted versus many initial concentrations of superoxide, we observed an increase in the concentration of $O_2^{\bullet-}$ reacted which reached a plateau at a value approximately equal to the total enzyme concentration of 3.9 μM (Figure 4). This suggests that the extent of inhibition of W161F Mn(II)SOD is nearly complete with the consumption of a concentration of superoxide equivalent to the concentration of this reduced enzyme.

W161F MnSOD is purified with manganese predominantly in the oxidized form, as determined from its absorption at 480 nm ($\epsilon \approx 600$ M^{-1} cm^{-1}). The data indicate that this mutant becomes inhibited after consuming about 2 molar equiv of $O_2^{\bullet-}$, one for the first half-cycle of the catalysis in which the metal is reduced (eq 1) followed by a second consumed by reaction of superoxide with reduced enzyme forming the inhibited complex (k_5 of eq 2). Thus it appears that a predominant pathway for the reaction of superoxide with W161F Mn(III)SOD proceeds through a half-cycle of catalysis, eq 1, and then forms an inhibited species.

To investigate further the kinetics and properties of these reactions, we repeated these experiments observing wave-

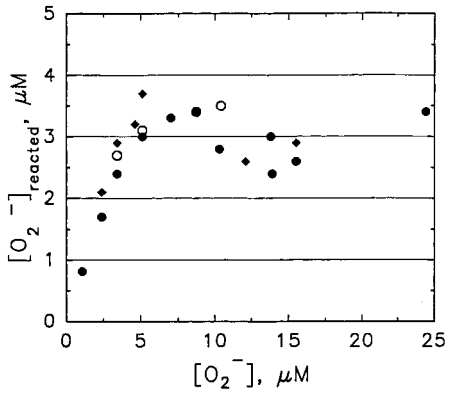

FIGURE 4: Concentration of superoxide reacted (μM) measured as a function of total superoxide in solution in the presence of the reduced enzyme W161F Mn(II)SOD (3.9 μM) at pH 7.2 (◆), pH 8.2 (○), and pH 9.2 (●). The following buffers were used: Mops (2.0 mM, pH 7.2), Taps (2.0 mM, pH 8.2), and Ches (2.0 mM, pH 9.2). Other conditions are as in Figure 2.

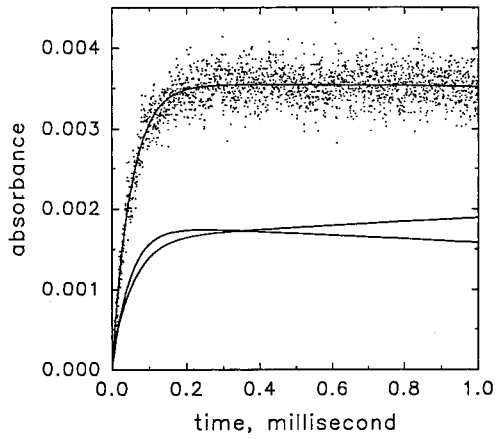

FIGURE 5: Increase in absorbance in the presence of 16 μM W161F MnSOD measured by pulse radiolysis at an initial concentration of superoxide of 1.0 μM at pH 8.2 in the presence of 2.0 mM Taps, 30 mM formate, and 50 μM EDTA at 25 °C. The enzyme sample was pretreated with 0.9 mM H_2O_2. The solid lines are least-squares fits to a first-order reaction with a linear (sloping) plateau with rate constants of (from top) 4.0×10^3 s^{-1} at 420 nm, 3.4×10^3 s^{-1} at 460 nm (slope trends up), and 4.3×10^3 s^{-1} at 380 nm (slope trends down). Experimental points are shown for just one experiment to simplify the figure.

lengths not of superoxide but of the enzyme itself. We reduced a large concentration of W161F MnSOD (16 μM) with an approximately 50-fold molar excess of H_2O_2 and then carried out pulse radiolysis to rapidly produce 1.0 μM $O_2^{\bullet-}$ while observing the visible absorption spectrum for the emergence of the oxidized enzyme or other transient species. The spectrum of W161F MnSOD in the presence of peroxide showed the expected lack of a visible spectrum, indicating that we had successfully reduced W161F MnSOD. Upon pulse radiolysis, we initially observed the spectrum of superoxide itself, emerging at wavelengths below 300 nm (data not shown). The subsequent kinetics were biphasic and widely separated in time. Figure 5 represents the initial reaction between W161F Mn(II)SOD and $O_2^{\bullet-}$ and Figure 6 represents the next phase of the reaction. As is apparent from the concentrations of the reactants given above, the initial reaction was measured under first-order conditions. At times extrapolated to completion of this reaction (Figure 5), the visible absorption spectrum showed a maximum at 420 nm with an apparent molar absorptivity of $\epsilon \approx 400-$

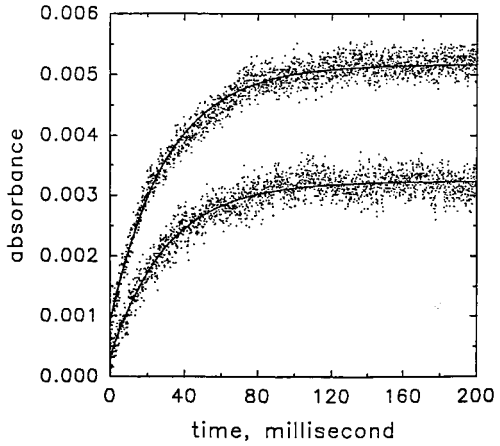

FIGURE 6: Increase in absorbance at (from top) 480 and 530 nm in the presence of 16 μM W161F MnSOD measured by pulse radiolysis at an initial concentration of superoxide of 1.0 μM at pH 8.2 in the presence of 2.0 mM Taps, 30 mM formate, and 50 μM EDTA at 25 °C. The enzyme sample was pretreated with 0.1 mM H_2O_2. The solid lines are least-squares fits to first-order kinetics to a plateau with rate constants of (from top) 31 s^{-1} and 33 s^{-1}.

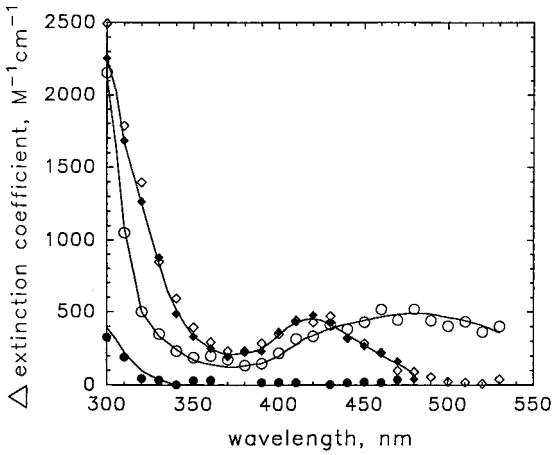

FIGURE 7: Change in extinction coefficient ϵ (M^{-1} cm^{-1}) as a function of wavelength upon pulse radiolysis of a solution of W161F MnSOD (16 μM) premixed with H_2O_2. Curves: (●) spectrum consistent with that of $O_2^{\bullet-}$ obtained by extrapolating the absorbance to the initial time in Figure 5; (◆) spectrum obtained from the plateau of the absorbance in Figure 5; (◇) spectrum obtained by extrapolating the absorbance to the initial time in Figure 6; (○) spectrum obtained from the plateau of the absorbance in Figure 6.

600 M^{-1} cm^{-1} (Figure 7, solid diamonds). This is the characteristic maximum and approximate value of the extinction coefficient determined for the product-inhibited state of the wild-type MnSOD (*5*). The emergence of the absorption at 420 nm in these experiments could be fit to first-order kinetics with a linear (sloping) plateau and a rate constant given in the legend of Figure 5. Dividing this rate constant by enzyme concentration gave an apparent second-order rate constant of 2.5×10^8 M^{-1} s^{-1}. Thus it appears that the oxidation of the reduced enzyme W161F Mn(II)-SOD by $O_2^{\bullet-}$ is fast and proceeds in large measure through a pathway that results in the product-inhibited complex that is relatively stable. One likely explanation is that the formation of the inhibited complex described by k_5 is faster than oxidation of the metal described by k_4. The decrease of the peak at 420 nm, representative of the inhibited complex, to a level consistent with the formation of the reduced enzyme was measured by scanning stopped-flow spectro-

photometry and could be fit to a first-order process with a rate constant of 24.4 ± 0.8 s^{-1}, under conditions of Figure 3 (data not shown).

The slow disappearance of the absorbance at 420 nm was explored in further experiments by mixing W161F MnSOD with H_2O_2. An approximately 6-fold molar excess of H_2O_2 was added to pretreat W161F Mn(III)SOD, and this solution was then used in the pulse radiolysis experiments (Figure 6). Here the decay of the absorbance at 420 nm, with the concomitant growth of an absorbance at 480 nm, was fitted to first-order kinetics. Extrapolation to the initial point again gave the absorbance characteristic of the product-inhibited state (Figure 7, open diamonds), and extrapolation to the completion of the reaction gave the spectrum with the absorption maximum at 480 nm characteristic of W161F Mn(III)SOD. The use of a lower concentration of H_2O_2 in these experiments reduced interference from the reduction of W161F Mn(III)SOD by peroxide, a much slower and, more importantly, second-order reaction that occurs with a rate constant that is proportional to peroxide concentration under these conditions. As the data here demonstrate, there is a pathway from the inhibited state to Mn(III)SOD, as suggested by Bull et al. (*5*) and earlier by McAdam et al. (*3*) and shown as k_{-5} of eq 2. The first-order increase from the initial low absorbance at 480 nm (due to the inhibited complex) to a plateau of absorbance at 480 nm [due to uninhibited oxidized enzyme W161F Mn(III)SOD] gave a rate constant near 31.0 ± 0.3 s^{-1} (Figure 6). This is to be compared with our value from stopped-flow (previous paragraph). The value of the rate constant for dissociation of the inhibited complex (corresponding to k_{-5} of eq 2) is estimated at 130 s^{-1} for wild-type human MnSOD at 20 °C by Hsu et al. (*4*) and 10 s^{-1} for *T. thermophilus* MnSOD at 2 °C. [Using a different and more simple model than eqs 1 and 2, McAdam et al. (*3*) found a value of 70 s^{-1} for *B. stearothermophilus* MnSOD at 25 °C.] Both McAdam et al. (*3*) and Bull et al. (*5*) show that the slope of the zero-order region of catalysis is directly proportional to k_{-5}. Hence, the smaller value of the rate constant for the decrease of the peak at 420 nm for W161F MnSOD (31 s^{-1}) is consistent with the data of Table 1 showing that this mutant appears to be more inhibited than wild type. However, it is important to point out that many of the rate constants of eqs 1 and 2 besides k_{-5} could also possibly contribute to the greater product inhibition of W161F MnSOD observed during the catalyzed dismutation of $O_2^{\bullet -}$. The observation of a smaller rate constant k_{-5} is neither necessary nor sufficient for greater product inhibition in the dismutation direction.

DISCUSSION

We have found that Trp 161 in human MnSOD is not essential for catalysis in the reduction half-cycle of eq 1. The conservative replacement of Trp 161 with Phe resulted in an enzyme with k_{cat}/K_m reduced by only 3-fold compared with wild type. Although we were not able to increase $[O_2^{\bullet -}]$ to a value greater than K_m, we can estimate a lower limit for k_{cat} at 10^3 s^{-1}, about 40-fold less than wild-type MnSOD (Table 1). Hence, the replacement Trp 161 → Phe caused rather modest decreases in catalytic activity, compared for example to the conservative replacement Gln 143 → Asn (Table 1). The side chain amide of Gln 143 is hydrogen bonded to the manganese-bound water; there is no such strong interaction known between Trp 161 and the manganese-bound water, although the oxygen of this water is about 5 Å from the plane of the indole ring of Trp 161.

The position of the side chain of Phe 161 in W161F MnSOD superimposes on that of Trp 161 in the wild type (Figure 1); the distance from the α carbon of residue 161 to the manganese is unchanged in the mutant. Moreover, there appear to be no significant changes in the backbone positions between the mutant and wild type. What has occurred in the mutant is a general tightening of the hydrogen-bonded chain from the metal-bound aqueous ligand to His 30 which is characterized by the shortening of several hydrogen bonds. This occurs in a segment of the hydrogen-bonded scheme that connects many side chains and solvent molecules in the active site. In this particular case, the segment altered involves Mn−aqueous ligand−Gln 143−Tyr 34−H_2O−His 30. The distance between the manganese and its aqueous ligand may have changed in W161F, increasing by approximately 0.2 Å in the mutant. The hydrogen bond distance between this metal-bound solvent molecule and the amide of Gln is decreased 0.6 Å in the mutant. It is interesting that there is no change in the hydrogen-bonded distance between the side chain amide of Gln 143 and the hydroxyl of Tyr 34; this hydrogen-bonded pair twist as a unit in the mutant so that the hydroxyl oxygen of Tyr 34 in the mutant is 1.2 Å closer to the metal and the amide of Gln 143 is approximately 0.3 Å closer to the metal. The hydroxyl of Tyr 34 is in turn hydrogen bonded through a single water molecule to the side chain imidazole of His 30, and this distance is smaller by 0.8 Å in the mutant. These features are summarized in the following scheme in which the changes in distances between side chains and metal-bound solvent caused by the replacement Trp 161 → Phe are given.

$$\mathrm{Mn} \overset{+0.2\ \text{Å}}{\text{——}} \mathrm{solvent} \overset{-0.6\ \text{Å}}{\text{——}} \mathrm{Gln\ 143} \overset{0}{\text{—}} \mathrm{Tyr\ 34} \overset{-0.8\ \text{Å}}{\text{——}} \mathrm{His\ 30}$$

It is intriguing that these changes have relatively small effects on the catalysis of the dismutation of superoxide for the mutant compared with wild type (Table 1). The bigger change, however, is in the 10-fold greater product inhibition in the mutant. This suggests that the tighter hydrogen-bonding scheme in W161F may also provide stronger binding of product peroxide in the active site and hence a smaller rate of dissociation of product.

It may be meaningful that the two most inhibited mutants of human MnSOD studied to date (see Table 1) have significant alterations to Tyr 34, specifically W161F in which the hydroxyl of Tyr 34 is 1.2 Å closer to the metal compared with the wild type and Y34F. It is known that azide when bound to the metal of Mn(III)SOD of *T. thermophilus* causes an expansion of the coordination geometry to octahedral with the metal-bound azide hydrogen bonded to the hydroxyl of Tyr 34 (*26*). The similarities between the visible absorption spectrum of MnSOD inhibited by azide and the product-inhibited complex have been reported (*9*). Hence, the association of product inhibition with alteration of the orientation or mutation of Tyr 34 supports a role for this residue in promoting the release of product from MnSOD perhaps through proton transfer.

We have taken advantage of the greater inhibition of W161F MnSOD during catalysis to comment further on the

nature of this product inhibition. W161F Mn(III)SOD appears to consume approximately 2 molar equiv of $O_2^{\bullet-}$ to produce the inhibited state (Figure 4). That is, the initial half-reaction of eq 1 appears to occur followed not predominantly by the second half-cycle of eq 2 but mainly by a reaction in which $O_2^{\bullet-}$ and enzyme form an inhibited complex. So favorable is the formation of this inhibited state that, for the most part, the reactants W161F Mn(II)SOD and $O_2^{\bullet-}$ proceed directly to the product-inhibited form; that is, the catalytic burst is attributed to the first half-cycle and the subsequent consumption of $O_2^{\bullet-}$ yields the inhibited complex. The oxidation of the manganese in W161F MnSOD by superoxide appears mainly to proceed through the inhibited complex ($k_5 > k_4$); however, in the wild-type human MnSOD, complex formation appears more competitive with direct oxidation ($k_4 \approx k_5$) (*4*). In contrast, for *T. thermophilus*, k_4 is approximately 40 times faster than k_5 (*5*).

Since the superoxide dismutases must catalyze both the oxidation and reduction of their substrate, there is an upper and lower limit on the values of $E°$ (approximately -0.16 and $+0.89$ V) that can sustain catalysis, with SOD's in the middle of this range (*2*, *27*). The observation that W161F Mn(III)SOD can react with $O_2^{\bullet-}$ to yield Mn(II)SOD nearly as fast as in wild type suggests that the value of $E°$ for this mutant is still favorable for the half-cycle involving reduction of the manganese (eq 1). But since we are not observing the catalysis of the oxidation half-cycle (eq 2), we cannot comment that $E°$ is unchanged compared to wild type. That is, $E°$ for the mutant allows eq 1 but could possibly be too positive to allow the oxidation of metal in the half-cycle of eq 2.

Conclusion. Tryptophan 161 that forms a hydrophobic side of the active site cavity of human MnSOD is not essential for the reduction half-cycle of superoxide decay (eq 1). Its replacement with Phe resulted in modest decreases, about 3-fold, in the steady-state constant k_{cat}/K_m for the catalysis. The crystal structure shows the side chain of Phe 161 in the mutant superimposed on the position of the larger side chain of Trp 161 in the wild type; in addition, there are other changes in the active site which result in the strengthening of several hydrogen bonds connecting residues and water including the manganese-bound water. This is accompanied by a conformational change of Tyr 34, the side chain hydroxyl of which is 1.2 Å closer to the metal in the mutant. Intriguingly, what has occurred in the mutant is a 10-fold enhancement of product inhibition compared with that of the wild type. This suggests that a significant role of Trp 161 in the active site is to promote the dissociation of product peroxide.

ACKNOWLEDGMENT

We thank Dr. Chingkuang Tu for his guidance, helpful discussions, and assistance in many aspects of this work. We are pleased to acknowledge the technical assistance of Ms. Kristi Totten.

REFERENCES

1. Cabelli, D. E., Riley, D., Rodriguez, J. A. A., Valentine, J. S., and Zhu, H. (1999) in *Biomimetic Oxidations Catalyzed by Transition Metal Complexes* (Meunier, B., Ed.) Chapter 10, Imperial College Press, London (in press).
2. Holm, R. H., Kenepohl, P., and Solomon, E. I. (1996) *Chem. Rev. 96*, 2239−2314.
3. McAdam, M. E., Fox, R. A., Lavelle, F., and Fielden, E. M. (1977) *Biochem. J. 165*, 71−79.
4. Hsu, J. L., Hsieh, Y., Tu, C. K., O'Connor, D., Nick, H. S., and Silverman, D. N. (1996) *J. Biol. Chem. 271*, 17687−17691.
5. Bull, C., Niederhoffer, E. C., Yoshida, T., and Fee, J. A. (1991) *J. Am. Chem. Soc. 113*, 4069−4076.
6. Borgstahl, G. E. O., Parge, H. E., Hickey, M. J., Beyer, W. F., Hallewell, R. A., and Tainer, J. A. (1992) *Cell 71*, 107−118.
7. Borders, C. L., Bjerrum, M. J., Schirmer, M. A., and Oliver, S. G. (1998) *Biochemistry 37*, 11323−11331.
8. Sorkin, D. L., Duong, D. K., and Miller, A.-F. (1997) *Biochemistry 36*, 8202−8208.
9. Whittaker, M. M., and Whittaker, J. W. (1997) *Biochemistry 36*, 8923−8931.
10. Hunter, T., Ikebukuro, K., Bannister, W. H., Bannister, J. V., and Hunter, G. J. (1997) *Biochemistry 36*, 4925−4933.
11. Guan, Y., Hickey, M. J., Borgstahl, G. E. O., Hallewell, R. A., Lepock, J. A., O'Connor, D., Hsieh, Y., Nick, H. S., Silverman, D. N., and Tainer, J. A. (1998) *Biochemistry 37*, 4722−4730.
12. Hsieh, Y., Guan, Y., Tu, C. K., Bratt, P. J., Angerhofer, A., Lepock, J. R., Hickey, M. J., Tainer, J. A., Nick, H. S., and Silverman, D. N. (1998) *Biochemistry 37*, 4731−4739.
13. Beck, Y., Oren, R., Amit, B., Levanon, A., Gorecki, M., and Hartman, A. J. (1987) *Nucleic Acids Res. 15*, 9076.
14. Carlioz, A., and Touati, D. (1986) *EMBO J. 5*, 623−630.
15. Beck, B. A., Bartfield, D., Yavin, Z., Levanon, A., Gorecki, M., and Hartman, J. R. (1988) *Biotechnology 6*, 930−935.
16. Otwinowski, Z., and Minor, W. (1997) *Methods Enzymol. 276*, 307−326.
17. Brünger, A. T., Adams, P. D., Clore, G. M., DeLano, W. L., Gros, P., Grosse-Kunstleve, R. W., Jiang, J. S., Kuszewski, J., Nilges, M., Pannu, N. S., Read, R. J., Rice, L. M., Simonson, T., and Warren, G. L. (1998) *Acta Crystallogr. D54*, 905−921.
18. McRee, D. E. (1992) *J. Mol. Graphics 10*, 44−47.
19. Brünger, A. T., Kuriyan, J., and Karplus, M. (1987) *Science 235*, 458−460.
20. Buxton, G. V., Greenstock, C. L., Helman, L. P., and Ross, A. B. (1988) *J. Phys. Chem. Ref. Data 17*, 678.
21. Schwarz, H. A. (1981) *J. Chem. Educ. 58*, 101−105.
22. Rabani, J., and Nielson, S. O. (1969) *J. Phys. Chem. 73*, 3736−3744.
23. McClune, G. J., and Fee, J. A. (1978) *Biophys. J. 24*, 65−69.
24. McAdam, M. E., Lavelle, F., Fox, R. A., and Fielden, E. M. (1977) *Biochem. J. 165*, 81−97.
25. Yamakura, F., Rardin, R. L., Petsko, G. A., Ringe, D., Hiraoka, B. Y., Nakayama, K., Fujimura, T., Taka, H., and Murayama, K. (1998) *Eur. J. Biochem. 253*, 49−56.
26. Lah, M. S., Dixon, M. M., Pattridge, K. A., Stallings, W. C., Fee, J. A., and Ludwig, M. L. (1995) *Biochemistry 34*, 1646−1660.
27. Vance, C. K., and Miller, A.-F. (1998) *J. Am. Chem. Soc. 120*, 461−467.

BI9909142